



Article

Electrodes Based on Carbon Aerogels Partially Graphitized by Doping with Transition Metals for Oxygen Reduction Reaction

Abdalla Abdelwahab ^{1,†}, Jesica Castelo-Quibén ¹, José F. Vivo-Vilches ^{1,‡}, María Pérez-Cadenas ², Francisco J. Maldonado-Hódar ¹, Francisco Carrasco-Marín ¹  and Agustín F. Pérez-Cadenas ^{1,*} 

¹ Carbon Materials Research Group, Department of Inorganic Chemistry, Faculty of Sciences, University of Granada, Campus Fuentenueva s/n, ES18071-Granada, Spain; abdalla.abdelwahab85@gmail.com (A.A.); jescicacastelo@ugr.es (J.C.-Q.); joseviv@ugr.es (J.F.V.-V.); fmaldon@ugr.es (F.J.M.-H.); fmarin@ugr.es (F.C.-M.)

² Department of Inorganic and Technical Chemistry, Science Faculty, UNED, Paseo Senda del Rey 9, ES28040-Madrid, Spain; mariaperez@ccia.uned.es

* Correspondence: afperez@ugr.es; Tel.: +34-958-243-316

† Present address: Material Science and Nanotechnology Department, Faculty of Postgraduate Studies for Advanced Science, Beni-Suef University, Beni-Suef 62511, Egypt.

‡ Present address: Laboratoire de Chimie Physique et Microbiologie pour l'Environnement, UMR 7564 CNRS, 54600 Villers-lès-Nancy, France.

Received: 18 April 2018; Accepted: 20 April 2018; Published: 23 April 2018



Abstract: A series of carbon aerogels doped with iron, cobalt and nickel have been prepared. Metal nanoparticles very well dispersed into the carbon matrix catalyze the formation of graphitic clusters around them. Samples with different Ni content are obtained to test the influence of the metal loading. All aerogels have been characterized to analyze their textural properties, surface chemistry and crystal structures. These metal-doped aerogels have a very well-developed porosity, making their mesoporosity remarkable. Ni-doped aerogels are the ones with the largest surface area and the smallest graphitization. They also present larger mesopore volumes than Co- and Fe-doped aerogels. These materials are tested as electro-catalysts for the oxygen reduction reaction. Results show a clear and strong influence of the carbonaceous structure on the whole electro-catalytic behavior of the aerogels. Regarding the type of metal doping, aerogel doped with Co is the most active one, followed by Ni- and Fe-doped aerogels, respectively. As the Ni content is larger, the kinetic current densities increase. Comparatively, among the different doping metals, the results obtained with Ni are especially remarkable.

Keywords: carbon aerogel; graphitic cluster; metal nanoparticle; oxygen reduction reaction; electro-catalysis

1. Introduction

Nowadays the development of electric vehicles is one of the most promising alternatives to replace combustion engines and therefore there is a high interest in finding new environmental friendly sources of energy for automotive applications. For this reason, the production of electrical energy from chemical reactions by using fuel cells is a really interesting matter from both the industrial and fundamental research points of view [1–3]. Oxygen Reduction Reaction (ORR) takes place on the cathode in a fuel cell and several works can be found in the published literature about the synthesis and optimization of electro-catalytic materials for this reaction [1–11]. Of these, platinum-based electro-catalysts happen to be the most widely studied, since Pt is the most active metal for ORR [1,6–10]. Nevertheless, the rising price of platinum and other precious metals as Pd or Ir makes it more difficult to commercialize devices

containing them. This is the reason why non precious metal electro-catalysts are more numerous and more studied in order to lower the costs of fuel cells [2,5–12].

On the other hand, carbon-based materials are being seriously considered as optimal candidates for ORR electro-catalysts [2,11,13,14]. Carbon gels are nanostructured materials, they are obtained from organic gels after their carbonization. Organic gels are prepared by polycondensation of organic monomers, normally resorcinol (R) and formaldehyde (F) [15]. The textural characteristics of carbon gels strongly depend on a precise control of the reactant concentrations and the conditions of the synthesis process: gelation, curing, drying and carbonization [16–18]. Surfactants can be added during the R-F polymerization which influences the morphology of the doped carbon gels and the metal dispersion [19]. Both surface area and pore volume, including the pore size distribution, are properties related to the synthesis conditions and processing that can be tuned, enabling the development of a wide set of materials with remarkable properties, e.g., for adsorption [20,21], catalysis [22–25] and electrochemical applications [26,27]. Besides, carbon gels doped with transition metals exhibit a homogeneous distribution together with a high dispersion of the metals throughout the carbon matrix [28,29]. Thus, transition metals are used in order to be anchored into the carbon matrix, which minimizes their leaching in liquid phase applications [19].

In the present work, carbon aerogels doped with iron, cobalt, and nickel were prepared, including a different nickel loading, exhaustibly characterized from textural, chemical, and electro-chemical points of view. Finally, their performances as electro-catalysts for the oxygen reduction reaction were evaluated and discussed in terms of their differences in porous texture, chemical characteristics, and metal doping, being the results of this comparative study the main objective of this work.

2. Materials and Methods

2.1. Preparation and Characterization of the Materials

Carbon aerogels doped with Ni, Co and Fe were prepared from resorcinol (R) and formaldehyde (F) dissolved in water (W) and using nickel, cobalt, or iron acetate as a catalyst precursor (C). The molar ratios were R:F = 1:2 and R:W = 1:17. Fe- and Co-doped aerogels were prepared only with a 6 wt %, approx. of metal loading while Ni-doped aerogels were prepared with 1, 4 and 6 wt %, approx. varying the amount of C. When an organic sol-gel solution was obtained it was cast into glass molds. After that, the curing process to obtain the organic gels was: 1 day at 40 °C, and 5 days at 80 °C. The glass molds were broken, and the organic aerogels were immersed in acetone for 24 h. Finally, the organic aerogels were treated with supercritical CO₂ for their drying. Another sample (A0), to be used as reference, was also prepared but without any transition metal. The organic aerogels were carbonized at 900 °C to obtain the carbon gels using a N₂ flow and a heating rate of 1 °C min^{−1}. The obtained carbon aerogels (A) were named as: ANi1, ANi4, ANi6, AFe6 and ACo6, the numbers indicate the approximate metal content in percentage. The metal loadings of the aerogels were determined by burning off a portion of a sample at 900 °C in air and weighting the residue.

The aerogels were texturally characterized by gas adsorption, scanning electron microscopy (SEM), and high-resolution transmission electron microscopy (HRTEM), and chemically characterized by X-ray diffraction (XRD), Raman spectroscopy and X-ray photoelectron spectroscopy (XPS). Samples performance for Oxygen Reduction Reaction was tested by means of cyclic voltammetry (CV) and linear sweep voltammetry (LSV).

N₂ and CO₂ adsorptions were carried out at −196 °C and 0 °C, respectively. Prior to measuring, the samples were outgassed for 24 h at 110 °C under high vacuum (10^{−6} mbar). The BET equation was applied to the N₂ adsorption obtaining the apparent surface area, S_{BET} . The Dubinin-Radushkevich (DR) equation was applied to the N₂ and CO₂ adsorption data and the corresponding micropore volume (W_0) and micropore mean width (L_0) were obtained. Total pore volumes ($V_{0.95}$) were determined from the N₂ adsorption isotherms at −196 °C and at 0.95 relative pressure. Finally,

the mesopore volumes (V_{BJH}) and the mean mesopore widths (L_{BJH}) were obtained applying the BJH method [30] to the desorption branch of the N_2 isotherms.

SEM was carried out using a Zeiss SUPRA40VP scanning electron microscope (Carl Zeiss AG, Oberkochen, Germany), equipped with a secondary electron detector, back-scatter electron detector, and using a X-Max 50 mm energy dispersive X-ray microanalysis system. All the samples were crushed before realizing this analysis.

HRTEM was performed using a FEI Titan G2 60-300 microscope (FEI, Eindhoven, The Netherlands) with a high brightness electron gun (X-FEG) operated at 300 kV and equipped with a Cs image corrector (CEOS) and for analytical electron microscopy (AEM) a SUPER-X silicon-drift window-less EDX detector. The AEM spectra were collected in STEM (scanning transmission electron microscopy) mode using a HAADF (high angle annular dark field) detector. Digital X-ray maps were also collected on selected areas of the samples.

Raman spectra were recorded using a Micro-Raman JASCO NRS-5100 dispersive spectrometer (JASCO Inc, Easton, MD, USA) with a 532 nm laser line. From these spectra the ratio $I_{\text{G}}/I_{\text{D}}$ was calculated as the quotient between the maximum intensity of each band.

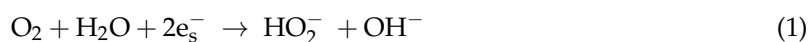
XRD analysis was carried out with BRUKER D8 ADVANCE diffractometer (BRUKER, Rivas-Vaciamadrid, Spain) using CuK radiation. JCPDS files were used to assign the different diffraction peaks observed. Diffraction patterns were recorded between 10° and 70° (2θ) with a step of 0.02° and a time per step of 96 s. The average crystal size (d_{XRD}) was determined using the Scherrer equation.

XPS measurements of the carbon aerogels were performed using a Physical Electronics ESCA 5701 (PHI, Chanhassen, MN, USA) equipped with a MgK X-ray source ($h\nu = 1253.6$ eV) operating at 12 kV and 10 mA, and a hemispherical electron analyzer. The obtained binding energy (BE) values were referred to the $\text{C}_{1\text{s}}$ peak at 284.7 eV. A base pressure of 10^{-9} mbar was maintained during data acquisition. Survey and multi-region spectra were recorded at $\text{C}_{1\text{s}}$, $\text{O}_{1\text{s}}$, $\text{Fe}_{2\text{p}}$, $\text{Co}_{2\text{p}}$ and $\text{Ni}_{2\text{p}}$ photoelectron peaks. Each spectral region was scanned enough times to obtain adequate signal-to-noise ratios. The spectra obtained after a background signal correction were fitted to Lorentzian and Gaussian curves to obtain the number of components, the position of each peak and the peak areas.

2.2. Electro-Chemical Studies. Oxygen Reduction Reaction

Cyclic Voltammetry (CV) and Linear Sweep Voltammetry (LSV) experiments were conducted on a three-electrode cell controlled by a Biologic VMP multichannel potentiostat (Bio-Logic Spain, Barcelona, Spain). A Rotating Disk Electrode (RDE) Metrohm AUTOLAB RDE-2 with a 3 mm Glassy Carbon tip (Gomensoro S.A, Madrid, Spain) was used as a working electrode. 5 mg of electro-catalyst were suspended on 1 mL of a solution which contained Nafion (5%) and water in a 1:9 (*v:v*) ratio. Subsequently, 10 μL of this suspension were loaded on RDE tip and dried under an infrared lamp [14]. The glassy carbon electrode had been previously polished with 1, 0.3 and 0.05 μm alumina powder and sonicated in deionized water and ethanol. Ag/AgCl was chosen as a reference electrode and Pt-wire as a counter electrode. The three electrodes were immersed in a 0.1 M KOH (electrolyte) solution in water.

The oxygen reduction reaction may occur by two different pathways: one implies 2e_s^- transference and the formation of peroxide species (Equation (1)) which could damage the electro-catalytic layer which is not desirable; the other leads only to the formation of hydroxide and it occurs by a 4e_s^- (Equation (2)) which is the requested one.



CV experiments were carried out while N_2 or O_2 bubbled through the electrolyte solution during the measurements. The chosen potential window ranged from -0.8 to 0.4 V (at $5\text{ mV}\cdot\text{s}^{-1}$ and $50\text{ mV}\cdot\text{s}^{-1}$). LSV curves were obtained in O_2 -saturated 0.1 M KOH solutions at a different rotation

speed and sweeping voltage, from 0.4 to -0.8 V ($5 \text{ mV}\cdot\text{s}^{-1}$). Data were fitted to the Koutecky-Levich model (Equations (3) and (4)) in order to evaluate the electro-catalytic performance of the samples and the transferred electron number for each of them [14].

$$\frac{1}{j} = \frac{1}{j_k} + \frac{1}{B\omega^{0.5}} \quad (3)$$

$$B = 0.2nF(D_{O_2})^{2/3}\nu^{-1/6}C_{O_2} \quad (4)$$

where j , current density; j_k , kinetic current density; ω , rotation speed; F , Faraday constant; D_{O_2} , oxygen diffusion coefficient ($1.9 \times 10^{-5} \text{ cm}^2\cdot\text{s}^{-1}$); ν , viscosity ($0.01 \text{ cm}^2\cdot\text{s}^{-1}$); C_{O_2} , oxygen concentration ($1.2 \times 10^{-6} \text{ mol}\cdot\text{cm}^{-3}$).

3. Results

Table 1 collects the names and the textural properties of the samples. All carbon aerogels are microporous and mesoporous materials with significant mesopore volumes and BET surface areas. Aerogels doped with Ni have the highest surface areas and pore volumes among the metal-doped samples, specially the highest micropore volumes; among the Ni samples ANi6 is the most microporous material. In the opposite site, AFe6 has the lowest surface area and pore volumes. Aerogel A has textural properties comparable with the rest of samples.

Figure 1 shows the morphology of the samples studied by SEM. The structure of the carbon gels consist in a network formed by rounded particles with a different degree of fusion [31]; a very well-developed macroporous structure is also observed. No significant morphological differences are observed by SEM among the samples.

Table 1. Name, surface areas and pore volumes of the doped carbon gels.

Sample	S_{BET}	$W_0(\text{N}_2)$	$L_0(\text{N}_2)$	$W_0(\text{CO}_2)$	$L_0(\text{CO}_2)$	$V_{0.95}(\text{N}_2)$	$V_{\text{BJH}}(\text{N}_2)$	L_{BJH}
	$\text{m}^2\cdot\text{g}^{-1}$	$\text{cm}^3\cdot\text{g}^{-1}$	nm	$\text{cm}^3\cdot\text{g}^{-1}$	nm	$\text{cm}^3\cdot\text{g}^{-1}$	$\text{cm}^3\cdot\text{g}^{-1}$	nm
A0	700	0.276	1.20	0.249	1.06	1.21	0.89	19.8
ANi1	663	0.258	1.07	0.276	0.63	0.82	0.54	17.1
ANi4	685	0.268	0.96	0.280	0.63	0.71	0.46	16.9
ANi6	698	0.273	0.90	0.294	0.64	0.69	0.48	16.8
ACo6	589	0.230	1.00	0.181	0.57	0.65	0.40	14.1
AFe6	461	0.177	1.00	0.182	0.62	0.41	0.25	12.3

Regarding the metal phase characterization, HRTEM analysis indicate that metals are mainly embedded within the carbon matrix; metal particles are clearly shown in Figures 2 and 3, and these are very well dispersed throughout the aerogel texture. Moreover, metal particles are detected within a wide range of nanometric sizes (Figure 4). On the other hand, these metal nanoparticles have catalyzed a partial graphitization around them during the pyrolysis; this fact was observed in all cases. Good examples of these graphitic clusters are shown in Figure 2, aerogels ANi6 and AFe6. It should be noted that the above-mentioned graphitization was not observed in sample A by HRTEM. These graphite clusters in the doped carbon aerogel structure were also observed in other works [31,32] with Co, Fe and Ni as doping metals. This can also be detected by XRD as a wide signal at around 26° (2θ) (peak 002 of graphite, JCPDS card No. 41-1487) specially in the case of aerogels ACo6 and AFe6 (Figure 5), although this signal hardly can be observed in the Ni doped samples. This would indicate that the graphitic clusters in the Ni samples probably have mean crystallite sizes smaller than 4 nm or a very thin laminar form.

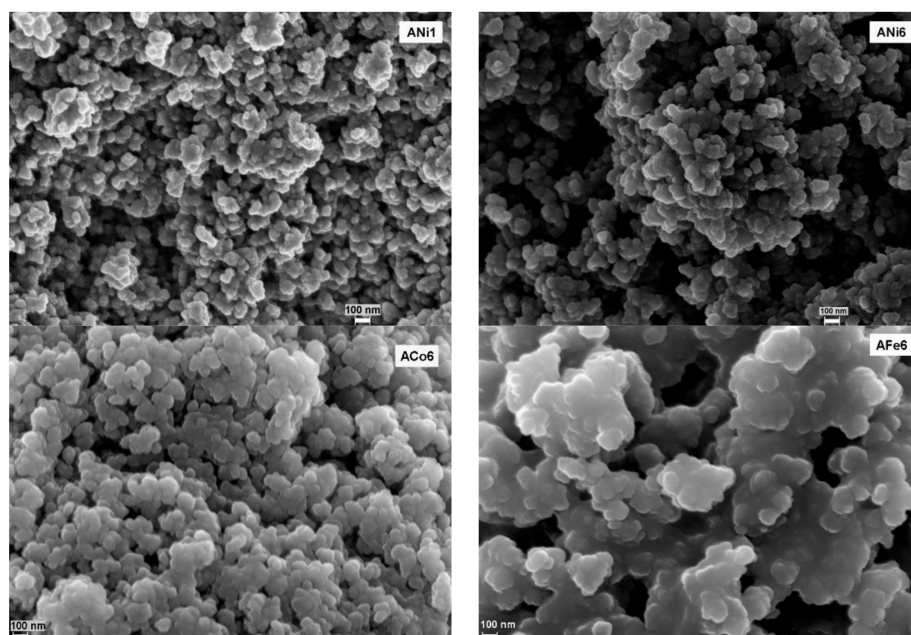


Figure 1. SEM microphotographs obtained at 100.00 KX of magnification of the samples ANi1, ANi6, ACo6 and AFe6.

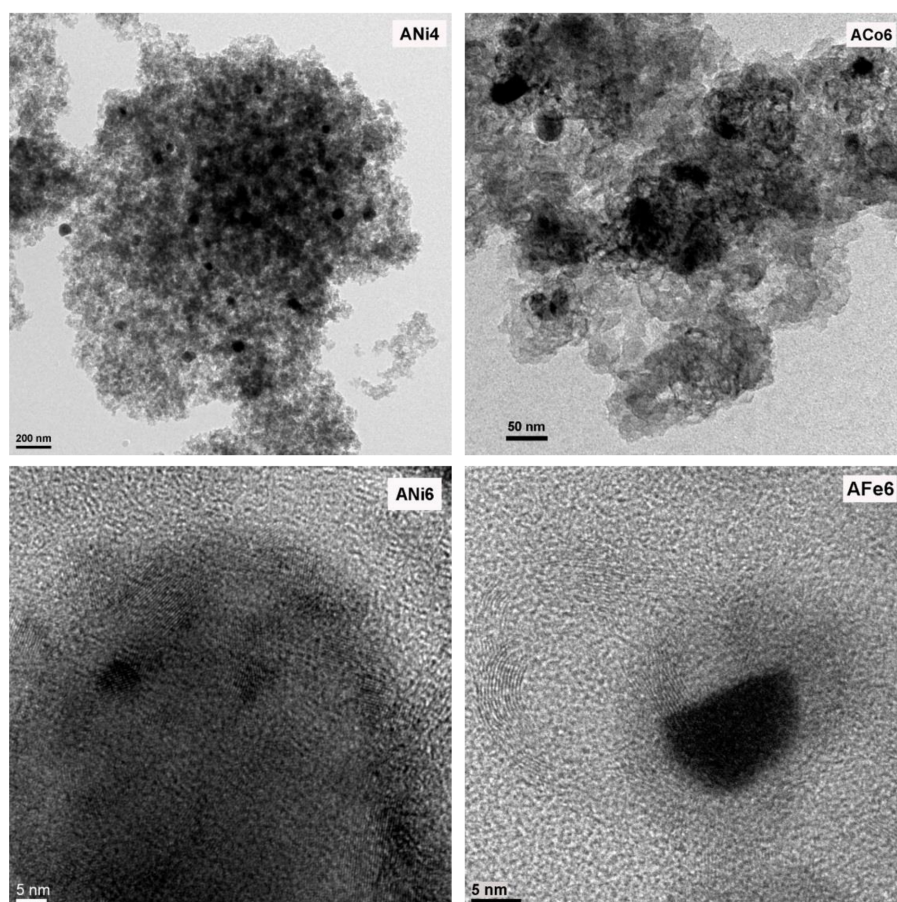


Figure 2. HRTEM images of the samples ANi4, ACo6, ANi6 and AFe6.

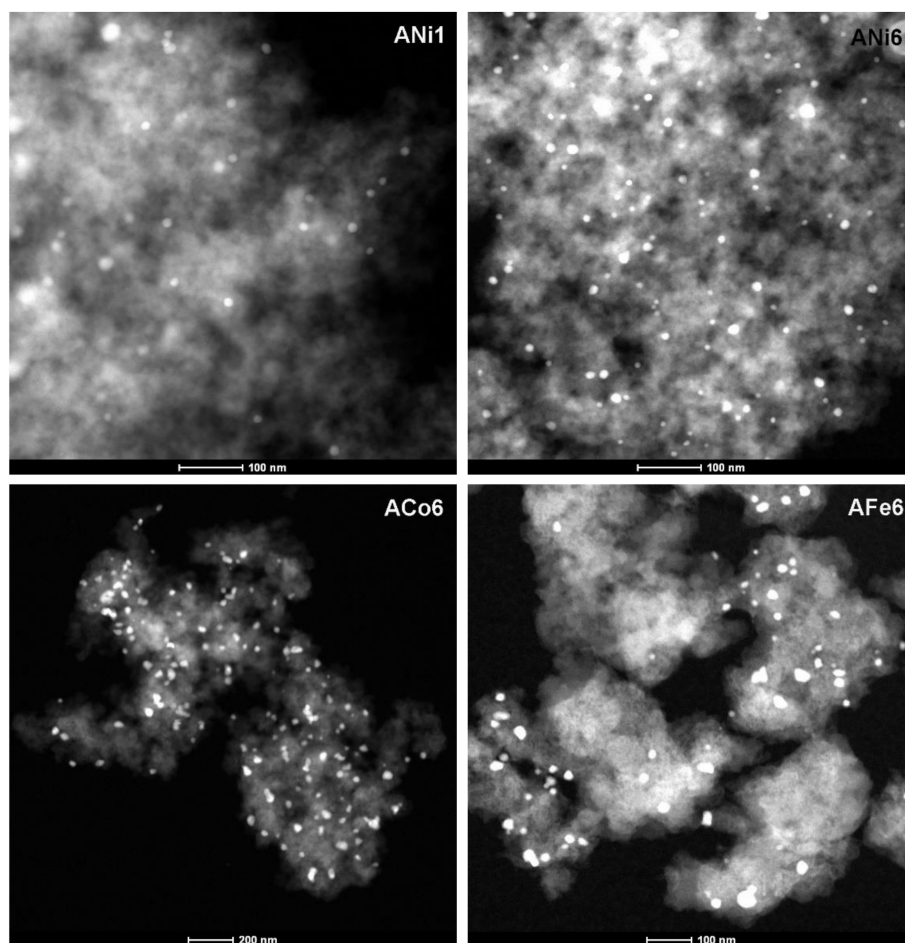


Figure 3. AEM spectra collected in STEM mode using a HAADF detector of the samples ANi1, ACo6, ANi6 and AFe6.

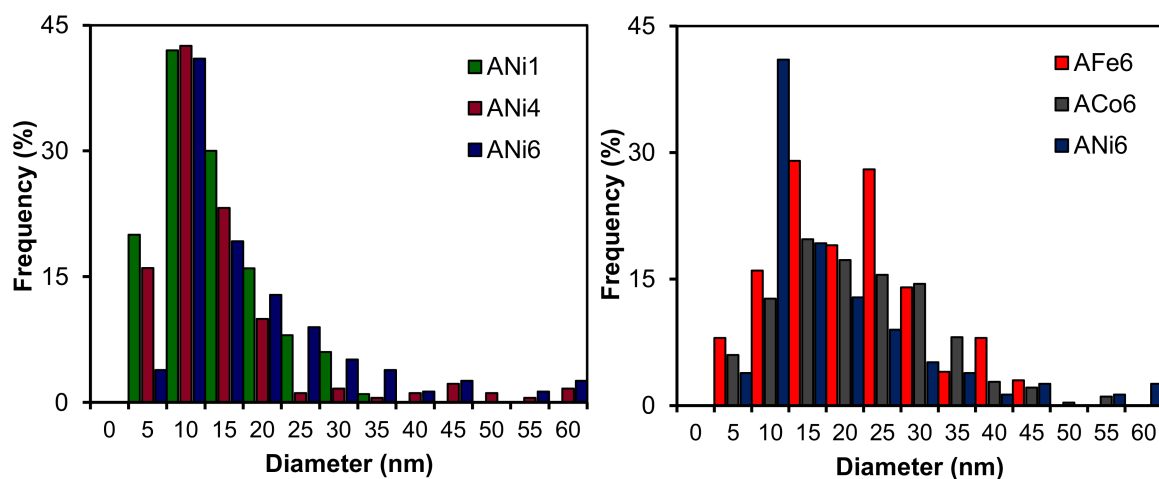


Figure 4. Particle size distributions obtained from HRTEM images.

On the other hand, the XRD peaks in Figure 5 clearly show the presence of Ni and Co completely reduced (JCPDS cards No. 04-0850, and 15-0806, respectively). Only in the case of sample AFe6 a mixture of Fe (0) (peaks at 44.6° and 65.1° , JCPDS card No. 06-0696) and Fe (III) (at 43.5°) could

be detected; although the coincidence of this signal with the peak (101) of graphite makes both its assignment and resolution, difficult.

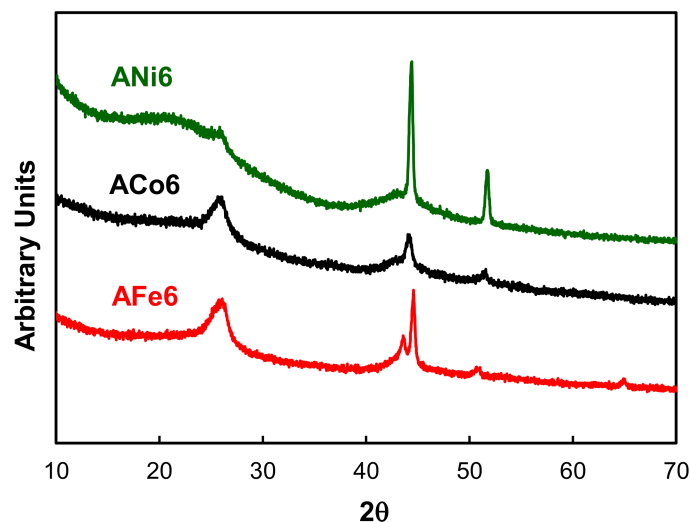


Figure 5. XRD patterns of aerogels ANi6, ACo6 and AFe6.

Analyzing the XP spectra, the peaks corresponding with metal phases cannot be practically distinguished from the base line in the case of ANi1 and ANi4, this means that Ni concentration on the external surface of these samples can be considered negligible. Only Ni2p, Co2p and Fe2p spectra of aerogels with 6 wt % could be analyzed. Figure 6 shows in the Ni2p spectrum only one Ni2p_{3/2} signal at 853.3 eV which is assigned to Ni (II) [33]; its corresponding satellite peak can be clearly observed at 859.8 eV. In this line, only one Co2p_{3/2} signal is observed at 781.1 eV of BE together its corresponding satellite at 786.1 eV, which is also assigned to Co (II) species [33]. Finally, the Fe2p spectrum contains two species of iron at 710.7 and 712.7 eV being these signals assigned to Fe₂O₃ (76.5%) and Fe₃O₄ (23.5%), respectively [33].

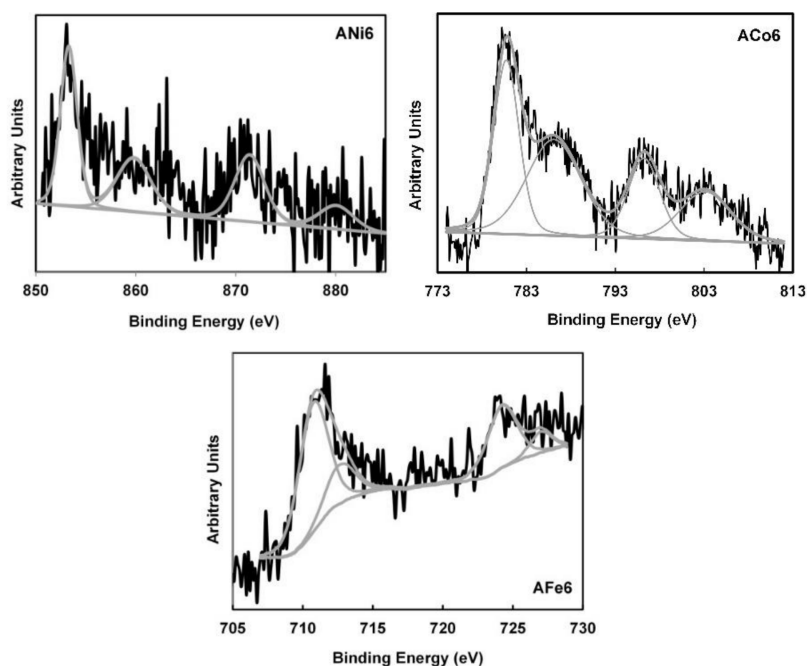


Figure 6. XP spectra of the doped carbon aerogels.

Raman spectra show (Figure 7) two main peaks at 1340 and 1580 cm^{-1} approx. which correspond to the D and G bands respectively [33]. In carbon aerogels, the D band can be associated with alternating ring vibrations in condensed benzene rings [34], while the G band can be associated with the development of the sp^2 carbon structure throughout the material during the carbonization process. It should be noted that carbon gels are normally amorphous carbon materials. Besides this, the intensity of the G band (I_G) with respect to its D band (I_D) is higher in the Ni doped aerogels than in the case of Fe or Co samples, and among the Ni samples this ratio I_G/I_D is clearly higher in ANi6 and ANi4 than in ANi1 (Table 2).

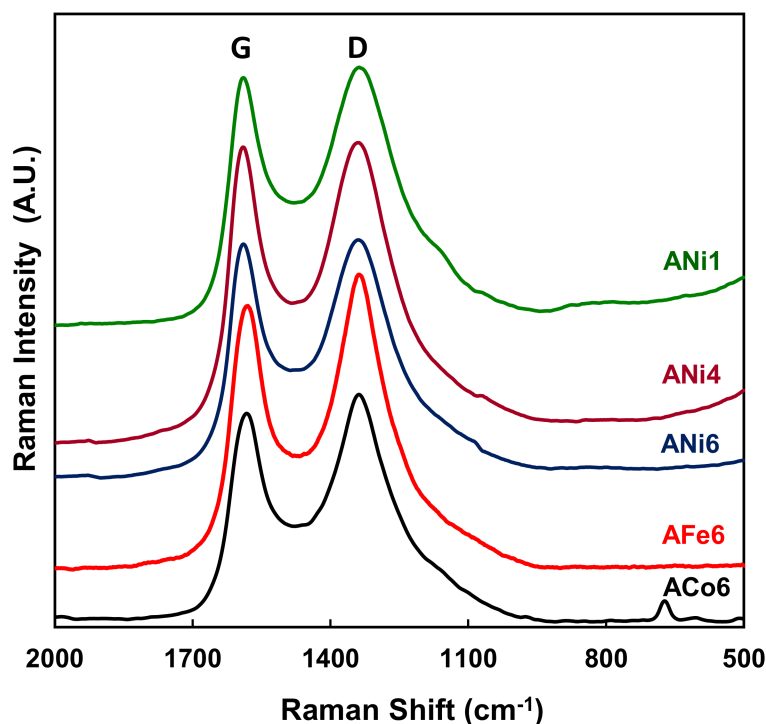


Figure 7. Raman spectra of the doped carbon aerogels.

Table 2. Chemical characteristics of the carbon aerogels.

Sample	Metal _{TOTAL} wt %	Metal _{XPS} wt %	O _{XPS} wt %	d_{XRD} nm	d_{HRTEM} nm	I_G/I_D
A0	n.d.	n.d.	1.4	n.d.	n.d.	-
ANi1	1.2	n.d.	1.6	15.9	11.9	0.97
ANi4	3.9	n.d.	1.6	17.4	15.5	0.99
ANi6	5.8	0.3	1.8	21.1	17.7	0.99
ACo6	5.9	0.7	3.6	21.5	19.4	0.92
AFe6	6.1	0.4	2.9	21.6	18.6	0.89

n.d.: no detected.

Table 2 collects the metal crystallite sizes estimated by applying the Scherrer equation, the mean particle sizes obtained from HRTEM, the I_G/I_D ration obtained from Raman spectra, the chemical composition obtained by XPS and total metal content of the aerogels. Among the Ni samples, the mean nickel particle size clearly increases with the metal loading; however, the samples ANi6, ACo6 and AFe6 show a very similar value around 21 nm.

Regarding the Rotating Disk Electrode (RDE) experiments, cyclic voltammetry was used in order to observe the difference between the samples behavior on a N_2 -saturated electrolyte (KOH 0.1 M) and an O_2 -saturated one. Figure 8 shows CV curves for ANi6 sample at 5 $\text{mV}\cdot\text{s}^{-1}$ and at 50 $\text{mV}\cdot\text{s}^{-1}$,

as well as for AFe6 and ACo6 samples at $50 \text{ mV}\cdot\text{s}^{-1}$ for comparison. In all cases a peak corresponding to the oxygen reduction can be observed when the curve is obtained on the O_2 -saturated electrolyte.

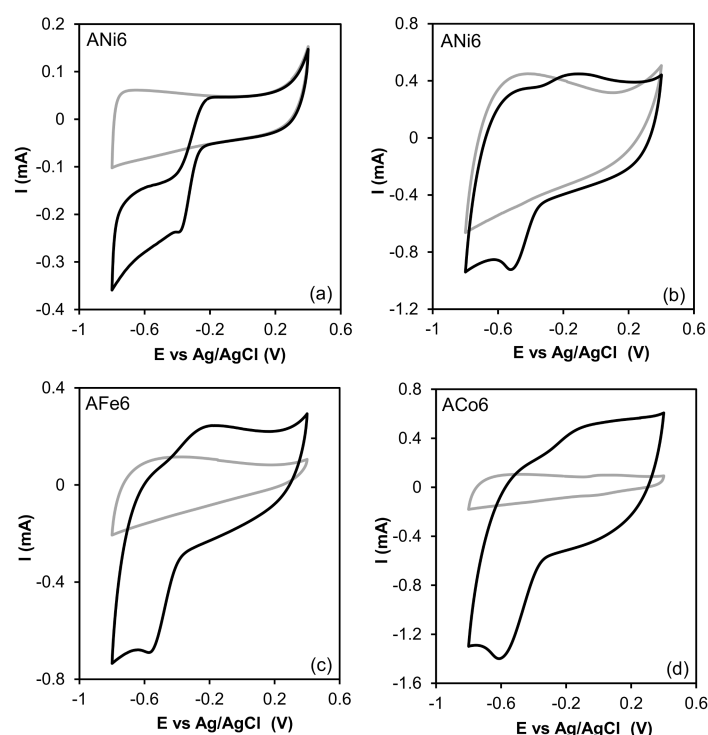


Figure 8. Cyclic voltammeteries on N_2 -saturated KOH 0.1 M (grey) and O_2 -saturated KOH 0.1 M (black). (a) $5 \text{ mV}\cdot\text{s}^{-1}$; (b–d) $50 \text{ mV}\cdot\text{s}^{-1}$.

After CV, the electro-catalytic performance of the samples for oxygen reduction was studied by Linear Sweep Voltammetry (LSV). The experiments were conducted at a different rotating speed to apply the Koutecky-Levich Equation. This analysis is shown in Figure 9 for the ANi6 sample.

From this analysis the number of electrons transferred at a given potential can be obtained (Table 3). Aerogels with different content in Ni were tested to analyze the influence of the metal content in the electro-catalytic behavior of the samples on LSV (Figure 10a) and the number of electrons transferred (Figure 10b). Finally, aerogels doped with the three different metals but with the same metal loading (ANi6, ACo6 and AFe6) were compared as well (Figure 11). None catalytic activity was detected with the un-doped aerogel A0, neither by CV nor LSV.

Table 3. Parameters obtained from the analysis of LSV curves (values of n refer to K-L fitting for data at -0.8 V).

Sample	E_{onset}	j_k	n
	V	$\text{mA}\cdot\text{cm}^{-2}$	
ANi1	−0.22	16.6	3.1
ANi4	−0.21	16.9	3.9
ANi6	−0.21	28.1	4.2
ACo6	−0.17	34.9	3.6
AFe6	−0.22	26.2	4.1

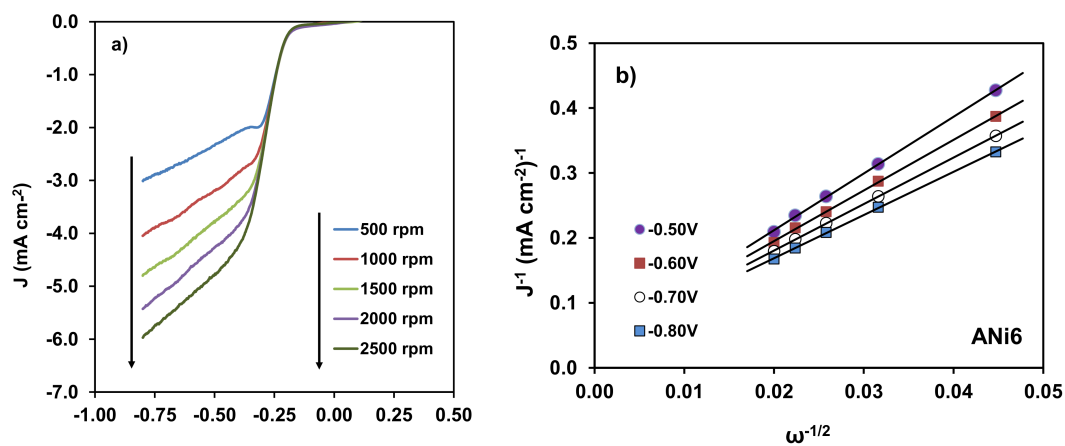


Figure 9. (a) LSV for ANi6 at different RDE rotating speed. (b) Koutecky-Levich fits at different potentials: from -0.5 to -0.8 V.

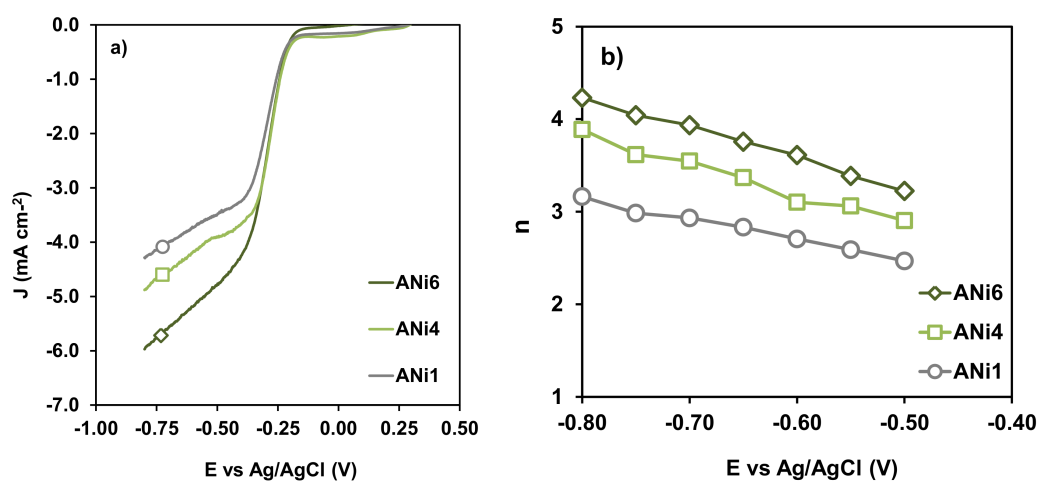


Figure 10. (a) LSV curves at 2500 rpm, and (b) variation of n with E vs. Ag/AgCl for samples ANi1 (○), ANi4 (□), ANi6 (◇).

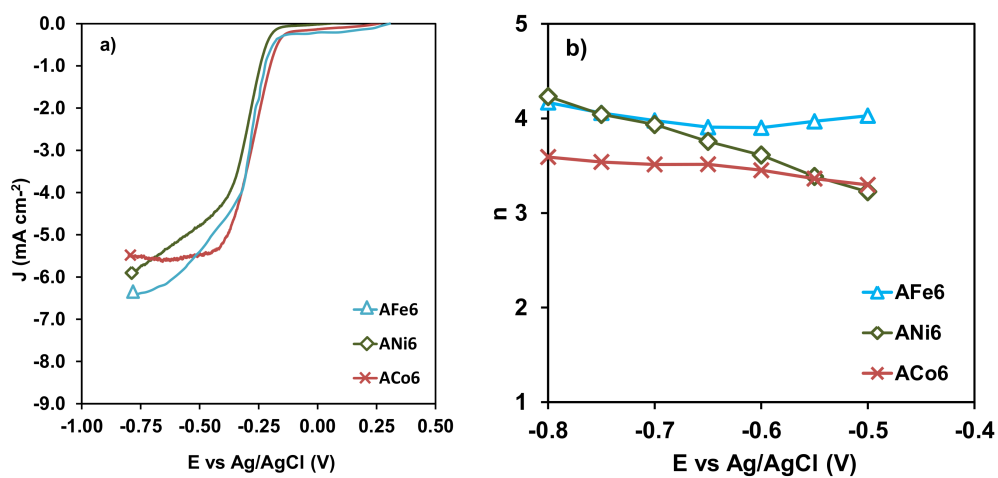


Figure 11. (a) LSV curves at 2500 rpm, and (b) variation of n with E vs. Ag/AgCl for samples AFe6 (Δ), ACo6 (×) and ANi6 (◇).

4. Discussion

After analyzing the textural data collected in Section 3, it is concluded that metal-doped aerogels contain a very well-developed porosity, especially with a significant mesoporosity (V_{BJH}). Aerogels doped with Ni have the highest surface areas and pore volumes, specially the highest micropore volumes. The metal phases are homogeneously distributed into the carbon matrix and well dispersed. Doped aerogels contain a wide range of sizes of metal nano-particles, most of them with a zero-oxidation state (those embedded in the carbon matrix), with the exception of sample AFe6, which shows a mixture of Fe (0) and Fe (III). On the other hand, very low percentages of metal particles are detected in the external non-porous surface area, which would be partially oxidized. The macro-structure of these aerogels is similar among the samples; however, a partial graphitization process around the metal particles has also been detected in the case of the three different metals. In this line carbon aerogels doped with Ni seem to have the smallest and the best-developed graphitic clusters since their I_G/I_D values are the highest [35], which could be due to the fact that they have the smallest metal particles (Figure 4 and Table 2).

Regarding electro-catalytic experiments, it can be observed that increasing the Ni loading improved the electro-catalytic performance of the aerogel (Figure 10). In fact, when the Ni percentage was really small (ANi1), the oxygen reduction reaction occurs through a combination of the 2 and 4 e^- , denoted by a value of $n = 3.1$ (Table 3). Nevertheless, as the Ni content increased, the number of electrons transferred also did, and the oxygen reduction occurred with an electronic transfer of 4 e^- s on both ANi4 and ANi6, although the reaction started at similar potentials as denoted by the value of E_{onset} (Table 3).

With respect to the type of metal, ACo6 is the best electro-catalyst showing the highest values of current density and the lowest value of E_{onset} among all the samples studied. On the other hand, some differences are also observed between ANi6 and AFe6 (Figure 11): ANi6 is the sample where the oxygen reduction occurs with a larger current density, although keeping the value of E_{onset} similar for both. According to bibliography [13,36,37], Ni-based electro-catalytic are in general less active than those-based in Fe or Co, this would be related to the ability of the metal to produce the dissociation of the oxygen molecule. However, in our material series, ANi6 show a very good electro-catalytic performance, even better than that for AFe6. In this case, ANi6 needs to be considered for its larger micropore volume and its smaller size of graphitic clusters. In fact, the electro-catalytic behavior of the carbon materials on the Oxygen Reduction Reaction is closely related to the type of carbon structure present in the material [38,39], and to its porosity. As was mentioned in previous paragraphs, the graphitic clusters for ANi6 are much smaller than those in the case of AFe6 and ACo6, therefore its good electro-catalytic performance could very well be related to it. In any case, it should be remarked that the catalytic results obtained with Ni-doped aerogels are especially interesting and much more in comparison to those obtained with Co- and Fe-doped ones.

On the other hand, we have included in Table 4 some bibliographic results obtained in similar experimental conditions to ours, and using as electro-catalysts Pt, Ni, Co, and Fe supported on different carbon materials. Pt/Carbon catalysts with a 20 wt % of Pt loading are a typical reference electrode [40–45], some authors use carbon black [40,43–45] and others prefer graphitic carbons as support [41,42]; in any case, all the collected results with this type of reference catalyst show the lowest E_{onset} potentials, which is reasonable because Pt itself is a better catalyst than the others, but the reported j_k values are lower or similar to ours. Despite that, our catalysts have much lower metal loadings and they do not contain platinum. Similar conclusions are obtained when carbon aerogels (prepared from melamine) [13,36], graphene oxide [46] or carbon nanotubes [44,45,47] were used as support of Ni, Co, or Fe; therefore, our j_k values are really good in comparison with those collected in Table 4. It is also remarkable that we have not found in the literature Ni-carbon-based electro-catalysts with a better performance than our ANi6 using similar ORR experimental conditions; its $j_k = 28.1$ is really significant. Thus, some electro-catalysts with low metal contents show n -values close to 2 which are lower than those obtained with our electro-catalysts ANi1 ($n = 3.1$). Finally, Ni and Co

unsupported nanoparticles [48] have been described as not catalytically active in this experimental ORR condition. These results, together with the fact that our un-doped A0 aerogel neither was active in the reaction, would indicate some type of catalytic synergism effect between the carbon and metal phases, especially taking in account that the accessibility of the metal particles to the electrolyte could be limited by the graphitic cluster developed around them.

Table 4. Comparison of our electro-catalysts with others found in the literature using similar conditions and electrolyte KOH 0.1 M.

Catalyst Name	Type of Support	E_{onset} vs. Ag/AgCl (V)	n	Ref.	Metal wt %	$j_k \text{ mA} \cdot \text{cm}^{-2}$
ANi6	Carbon aerogel	−0.210	4.2	This work	5.8	28.1
ACo6	Carbon aerogel	−0.170	3.6	This work	5.8	34.9
AFe6	Carbon aerogel	−0.220	4.1	This work	6.1	26.2
20% Pt Vulcan	Carbon black	−0.037	3.9	[40]	20	N.R.
20% Pt/C	Graphitic carbon	−0.050	3.9	[41]	20	5
20% Pt/C	Graphitic carbon	−0.070	4.2	[42]	20	28.8
20% Pt/C	Carbon black	−0.065	4.0	[43]	20	14
20% Pt/C	Carbon black	-	3.9	[44]	20	≈29 *
Pt/Vulcan	Carbon black	−0.007	3.9	[45]	20	N.R.
NT_FePc_400	Carbon nanotube	−0.037	3.9	[45]	2.1	N.R.
NT_CoPc_400	Carbon nanotube	−0.150	2.4	[45]	2.1	N.R.
Co-NCA	Carbon aerogel	−0.150	4.0	[36]	3	≈25 *
Fe-NCA	Carbon aerogel	−0.150	3.8	[36]	5.2	≈14 *
Fe-NCA5	Carbon aerogel	−0.051	3.8	[13]	7.7	≈25 *
FeCo-N-rGO	Carbon nanotube	0.050	3.9	[44]	0.46	≈25 *
CoNPs/rGO	Graphene oxide	−0.115	3.9	[46]	0.3	N.R.
Fe3C-CNTFs	Carbon nanotube	0.105	3.1	[47]	N.R.	4.89
Co-CNTFs	Carbon nanotube	−0.015	3.9	[47]	N.R.	5.23
Ni-CNTs	Carbon nanotube	0.055	2.6	[47]	N.R.	3.67
Ni	Unsupported	0	0	[48]	100	0
Co	Unsupported	0	0	[48]	100	0

(N.R.) j_k values or j^{-1} vs. $\omega^{-1/2}$ plots not reported; (*) Data estimated from the corresponding j^{-1} vs. $\omega^{-1/2}$ plots.

Therefore, the results of this work clearly show that carbon aerogels doped with transition metals (obtained by polymerization of resorcinol and formaldehyde) are very good candidates as oxygen reduction electro-catalysts, where the current densities depend on the type and amount of metal doping and where the role of the carbon phase, both its textural and chemical properties, have a strong influence on the whole catalytic behavior of the material.

5. Conclusions

All the metal-doped carbon aerogels showed promising behavior in the oxygen reduction reaction; their well-developed porosity together with a very good metal dispersion in the carbon matrix, lead to materials with a very high electro-catalytic activity in ORR. As the Ni content was increased, the electro-catalytic behavior improved. Co-doped aerogel is the best electro-catalyst, showing the highest values of current density and the lowest value of E_{onset} among all the studied samples. Nevertheless, the nickel-doped aerogel (ANi6) presented even better results than the Fe one, which can be very well related to changes in the carbon crystalline structure and porosity, since ANi6 is the aerogel with the largest micropore and mesopore volumes and also the one with the smallest graphitic clusters. In general, the presence of small and well-developed graphitic domains seems to improve the electro-catalytic reduction of oxygen.

Acknowledgments: This research is supported by the FEDER and Spanish projects CTQ2013-44789-R (MINECO) and P12-RNM-2892 (Junta de Andalucía). A.A. is grateful to the European Union for his Erasmus Mundus fellowship, Program ELEMENT. J. C.-Q. is grateful to the Junta de Andalucía for her research contract (P12-RNM-2892). We thank the “Unidad de Excelencia Química Aplicada a Biomedicina y Medioambiente” (UGR) for its technical assistance”.

Author Contributions: A.F.P.-C., M.P.-C. and F.C.-M. conceived and designed the experiments; A.A., J.C.-Q. and J.F.V.-V. performed the experiments; A.F.P.-C., F.C.-M., M.P.-C. and F.J.M.-H. analyzed the data; A.F.P.-C. and F.C.-M. wrote the paper.

Conflicts of Interest: The authors declare no conflict of interest.

References

1. Jung, D.H.; Bae, S.J.; Kim, S.J.; Nahm, K.S.; Kim, P. Effect of the Pt precursor on the morphology and catalytic performance of Pt-impregnated on Pd/C for the oxygen reduction reaction in polymer electrolyte fuel cells. *Int. J. Hydrog. Energy* **2011**, *36*, 9115–9122. [\[CrossRef\]](#)
2. Yang, Z.; Nie, H.; Chen, X.; Chen, X.; Huang, S. Recent progress in doped carbon nanomaterials as effective cathode catalysts for fuel cell oxygen reduction reaction. *J. Power Sources* **2013**, *236*, 238–249. [\[CrossRef\]](#)
3. Banham, D.; Ye, S.; Pei, K.; Ozaki, J.-I.; Kishimoto, T.; Imashiro, Y. A review of the stability and durability of non-precious metal catalysts for the oxygen reduction reaction in proton exchange membrane fuel cells. *J. Power Sources* **2015**, *285*, 334–348. [\[CrossRef\]](#)
4. Lee, C.L.; Chiou, H.P.; Syu, C.M.; Wu, C.C. Silver triangular nanoplates as electrocatalyst for oxygen reduction reaction. *Electrochem. Commun.* **2010**, *12*, 1609–1613. [\[CrossRef\]](#)
5. Bo, X.; Zhang, Y.; Li, M.; Nsabimana, A.; Guo, L. NiCo₂O₄ spinel/ordered mesoporous carbons as noble-metal free electrocatalysts for oxygen reduction reaction and the influence of structure of catalyst support on the electrochemical activity of NiCo₂O₄. *J. Power Sources* **2015**, *288*, 1–8. [\[CrossRef\]](#)
6. Stojmenović, M.; Momčilović, M.; Gavrilov, N.; Pašti, I.A.; Mentus, S.; Jokić, B.; Babić, B. Incorporation of Pt, Ru and Pt-Ru nanoparticles into ordered mesoporous carbons for efficient oxygen reduction reaction in alkaline media. *Electrochim. Acta* **2015**, *153*, 130–139. [\[CrossRef\]](#)
7. Zhao, A.; Masa, J.; Xia, W. Oxygen-deficient titania as alternative support for Pt catalysts for the oxygen reduction reaction. *J. Energy Chem.* **2014**, *23*, 701–707. [\[CrossRef\]](#)
8. Kim, J.H.; Chang, S.; Kim, Y.T. Compressive strain as the main origin of enhanced oxygen reduction reaction activity for Pt electrocatalysts on chromium-doped titania support. *Appl. Catal. B Environ.* **2014**, *158*–159, 112–118. [\[CrossRef\]](#)
9. Ahmed, M.S.; Kim, D.; Jeon, S. Covalently grafted platinum nanoparticles to multi walled carbon nanotubes for enhanced electrocatalytic oxygen reduction. *Electrochim. Acta* **2013**, *92*, 168–175. [\[CrossRef\]](#)
10. Oh, J.-M.; Park, J.; Kumbhar, A.; Smith, D.; Creager, S. Electrochemical Oxygen Reduction at Platinum/Mesoporous Carbon/Zirconia/Ionomer Thin-Film Composite Electrodes. *Electrochim. Acta* **2014**, *138*, 278–287. [\[CrossRef\]](#)
11. Dou, S.; Shen, A.; Ma, Z.; Wu, J.; Tao, L.; Wang, S. N-, P- and S-tridoped graphene as metal-free electrocatalyst for oxygen reduction reaction. *J. Electroanal. Chem.* **2015**, *753*, 21–27. [\[CrossRef\]](#)
12. Ishii, T.; Maie, T.; Kimura, N.; Kobori, Y.; Imashiro, Y.; Ozaki, J.-I. Enhanced catalytic activity of nanoshell carbon co-doped with boron and nitrogen in the oxygen reduction reaction. *Int. J. Hydrog. Energy* **2017**, *42*, 5–12. [\[CrossRef\]](#)
13. Sarapuu, A.; Kreek, K.; Kisand, K.; Kook, M.; Uibu, M.; Koel, M.; Tammeveski, K. Electrocatalysis of oxygen reduction by iron-containing nitrogen-doped carbon aerogels in alkaline solution. *Electrochim. Acta* **2017**, *230*, 81–88. [\[CrossRef\]](#)
14. Elmouwahidi, A.; Vivo-Vilches, J.F.; Pérez-Cadenas, A.F.; Maldonado-Hódar, F.J.; Carrasco-Marín, F. Free metal oxygen-reduction electro-catalysts obtained from biomass residue of the olive oil industry. *Chem. Eng. J.* **2016**, *306*, 1109–1115. [\[CrossRef\]](#)
15. Pekala, R.W.; Alviso, C.T.; Kong, F.M.; Hulsey, S.S. Aerogels derived from multifunctional organic monomers. *J. Non-Cryst. Solids* **1992**, *145*, 90–98. [\[CrossRef\]](#)
16. ElKhatat, A.M.; Al-Muhtaseb, S.A. Advances in tailoring resorcinol-formaldehyde organic and carbon gels. *Adv. Mater.* **2011**, *23*, 2887–2903. [\[CrossRef\]](#) [\[PubMed\]](#)
17. Gallegos-Suárez, E.; Pérez-Cadenas, A.F.; Maldonado-Hódar, F.J.; Carrasco-Marín, F. On the micro- and mesoporosity of carbon aerogels and xerogels. The role of the drying conditions during the synthesis processes. *Chem. Eng. J.* **2012**, *181*, 851–855. [\[CrossRef\]](#)

18. Morales-Torres, S.; Maldonado-Hódar, F.J.; Pérez-Cadenas, A.F.; Carrasco-Marín, F. Textural and mechanical characteristics of carbon aerogels synthesized by polymerization of resorcinol and formaldehyde using alkali carbonates as basification agents. *Phys. Chem. Chem. Phys.* **2010**, *12*, 10365–10372. [[CrossRef](#)] [[PubMed](#)]
19. Maldonado-Hódar, F.J.; Jirglová, H.; Pérez-Cadenas, A.F.; Morales-Torres, S. Chemical control of the characteristics of Mo-doped carbon xerogels by surfactant-mediated synthesis. *Carbon N. Y.* **2013**, *51*, 213–223. [[CrossRef](#)]
20. Vivo-Vilches, J.F.; Carrasco-Marín, F.; Pérez-Cadenas, A.F.; Maldonado-Hódar, F.J. Fitting the porosity of carbon xerogel by CO₂ activation to improve the TMP/n-octane separation. *Microporous Mesoporous Mater.* **2015**, *209*, 10–17. [[CrossRef](#)]
21. Maldonado-Hódar, F.J.; Moreno-Castilla, C.; Carrasco-Marín, F.; Pérez-Cadenas, A.F. Reversible toluene adsorption on monolithic carbon aerogels. *J. Hazard. Mater.* **2007**, *148*, 548–552. [[CrossRef](#)] [[PubMed](#)]
22. Bailón-García, E.; Carrasco-Marín, F.; Pérez-Cadenas, A.F.; Maldonado-Hódar, F.J. Microspheres of carbon xerogel: An alternative Pt-support for the selective hydrogenation of citral. *Appl. Catal. A Gen.* **2014**, *482*, 318–326. [[CrossRef](#)]
23. Bailón-García, E.; Elmouwahidi, A.; Álvarez, M.A.; Carrasco-Marín, F.; Pérez-Cadenas, A.F.; Maldonado-Hódar, F.J. New carbon xerogel-TiO₂ composites with high performance as visible-light photocatalysts for dye mineralization. *Appl. Catal. B Environ.* **2017**, *201*, 29–40. [[CrossRef](#)]
24. Duarte, F.; Maldonado-Hódar, F.J.; Pérez-Cadenas, A.F.; Madeira, L.M. Fenton-like degradation of azo-dye Orange II catalyzed by transition metals on carbon aerogels. *Appl. Catal. B Environ.* **2009**, *85*, 139–147. [[CrossRef](#)]
25. Maldonado-Hódar, F.J.; Moreno-Castilla, C.; Pérez-Cadenas, A.F. Catalytic combustion of toluene on platinum-containing monolithic carbon aerogels. *Appl. Catal. B Environ.* **2004**, *54*, 217–224. [[CrossRef](#)]
26. Elmouwahidi, A.; Bailón-García, E.; Pérez-Cadenas, A.F.; Maldonado-Hódar, F.J.; Castelo-Quibén, J.; Carrasco-Marín, F. Electrochemical performances of supercapacitors from carbon-ZrO₂ composites. *Electrochim. Acta* **2018**, *259*, 803–814. [[CrossRef](#)]
27. Elmouwahidi, A.; Bailón-García, E.; Castelo-Quibén, J.; Pérez-Cadenas, A.F.; Maldonado-Hódar, F.J.; Carrasco-Marín, F. Carbon-TiO₂ composites as high-performance supercapacitor electrodes: Synergistic effect between carbon and metal oxide phases. *J. Mater. Chem. A* **2018**, *6*. [[CrossRef](#)]
28. Pérez-Cadenas, A.F.; Maldonado-Hódar, F.J.; Moreno-Castilla, C. Molybdenum carbide formation in molybdenum-doped organic and carbon aerogels. *Langmuir* **2005**, *21*, 10850–10855. [[CrossRef](#)] [[PubMed](#)]
29. Maldonado-Hódar, F.J.; Pérez-Cadenas, A.F.; Moreno-Castilla, C. Morphology of heat-treated tungsten doped monolithic carbon aerogels. *Carbon N. Y.* **2003**, *41*, 1291–1299. [[CrossRef](#)]
30. Barrett, E.P.; Joyner, L.G.; Halenda, P.P. The determination of pore volume and area distributions in porous substances. I. Computations from nitrogen isotherms. *J. Am. Chem. Soc.* **1951**, *73*, 373–380. [[CrossRef](#)]
31. Maldonado-Hódar, F.J.; Moreno-Castilla, C.; Pérez-Cadenas, A.F. Surface morphology, metal dispersion, and pore texture of transition metal-doped monolithic carbon aerogels and steam-activated derivatives. *Microporous Mesoporous Mater.* **2004**, *69*, 119–125. [[CrossRef](#)]
32. Maldonado-Hódar, F.J.; Moreno-Castilla, C.; Rivera-Utrilla, J.; Hanzawa, Y.; Yamada, Y. Catalytic Graphitization of Carbon Aerogels by Transition Metals. *Langmuir* **2000**, *16*, 4367–4373. [[CrossRef](#)]
33. NIST X-ray Photoelectron Spectroscopy Database. Available online: <https://srdata.nist.gov/xps/> (accessed on 16 April 2018).
34. Schwan, J.; Ulrich, S.; Batori, V.; Ehrhardt, H.; Silva, S.R.P. Raman spectroscopy on amorphous carbon films. *J. Appl. Phys.* **1996**, *80*, 440. [[CrossRef](#)]
35. Wang, S.; Xu, Y.; Yan, M.; Zhai, Z.; Ren, B.; Zhang, L.; Liu, Z. Comparative study of metal-doped carbon aerogel: Physical properties and electrochemical performance. *J. Electroanal. Chem.* **2018**, *809*, 111–116. [[CrossRef](#)]
36. Sarapuu, A.; Samolberg, L.; Kreek, K.; Koel, M.; Matisen, L.; Tammeveski, K. Cobalt- and iron-containing nitrogen-doped carbon aerogels as non-precious metal catalysts for electrochemical reduction of oxygen. *J. Electroanal. Chem.* **2015**, *746*, 9–17. [[CrossRef](#)]
37. Chen, Z.; Higgins, D.; Yu, A.; Zhang, L.; Zhang, J. A review on non-precious metal electrocatalysts for PEM fuel cells. *Energy Environ. Sci.* **2011**, *4*, 3167–3192. [[CrossRef](#)]
38. Shin, D.; An, X.; Choun, M.; Lee, J. Effect of transition metal induced pore structure on oxygen reduction reaction of electrospun fibrous carbon. *Catal. Today* **2016**, *260*, 82–88. [[CrossRef](#)]

39. Chao, S.; Zhang, Y.; Wang, K.; Bai, Z.; Yang, L. Flower—like Ni and N codoped hierarchical porous carbon microspheres with enhanced performance for fuel cell storage. *Appl. Energy* **2016**, *175*, 421–428. [[CrossRef](#)]
40. Quílez-Bermejo, J.; González-Gaitán, C.; Morallón, E.; Cazorla-Amorós, D. Effect of carbonization conditions of polyaniline on its catalytic activity towards ORR. Some insights about the nature of the active sites. *Carbon N. Y.* **2017**, *119*, 62–71. [[CrossRef](#)]
41. Ferrero, G.A.; Preuss, K.; Fuertes, A.B.; Sevilla, M.; Titirici, M.-M. The influence of pore size distribution on the oxygen reduction reaction performance in nitrogen doped carbon microspheres. *J. Mater. Chem. A* **2016**, *4*, 2581–2589. [[CrossRef](#)]
42. Zhao, X.; Zhao, H.; Zhang, T.; Yan, X.; Yuan, Y.; Zhang, H.; Zhao, H.; Zhang, D.; Zhu, G.; Yao, X. One-step synthesis of nitrogen-doped microporous carbon materials as metal-free electrocatalysts for oxygen reduction reaction. *J. Mater. Chem. A* **2014**, *2*, 11666–11671. [[CrossRef](#)]
43. Pan, F.; Cao, Z.; Zhao, Q.; Liang, H.; Zhang, J. Nitrogen-doped porous carbon nanosheets made from biomass as highly active electrocatalyst for oxygen reduction reaction. *J. Power Sources* **2014**, *272*, 8–15. [[CrossRef](#)]
44. Fu, X.; Liu, Y.; Cao, X.; Jin, J.; Liu, Q.; Zhang, J. FeCo-Nx embedded graphene as high performance catalysts for oxygen reduction reaction. *Appl. Catal. B Environ.* **2013**, *130–131*, 143–151. [[CrossRef](#)]
45. González-Gaitán, C.; Ruiz-Rosas, R.; Morallón, E.; Cazorla-Amorós, D. Relevance of the Interaction between the M-Phthalocyanines and Carbon Nanotubes in the Electroactivity toward ORR. *Langmuir* **2017**, *33*, 11945–11955. [[CrossRef](#)] [[PubMed](#)]
46. Liu, X.; Yu, Y.; Niu, Y.; Bao, S.; Hu, W. Cobalt nanoparticle decorated graphene aerogel for efficient oxygen reduction reaction electrocatalysis. *Int. J. Hydrog. Energy* **2017**, *42*, 5930–5937. [[CrossRef](#)]
47. Wang, M.-Q.; Ye, C.; Wang, M.; Li, T.-H.; Yu, Y.-N.; Bao, S.-J. Synthesis of M (Fe₃C, Co, Ni)-porous carbon frameworks as high-efficient ORR catalysts. *Energy Storage Mater.* **2018**, *11*, 112–117. [[CrossRef](#)]
48. Goubert-Renaudin, S.N.S.; Wieckowski, A. Ni and/or Co nanoparticles as catalysts for oxygen reduction reaction (ORR) at room temperature. *J. Electroanal. Chem.* **2011**, *652*, 44–51. [[CrossRef](#)]



© 2018 by the authors. Licensee MDPI, Basel, Switzerland. This article is an open access article distributed under the terms and conditions of the Creative Commons Attribution (CC BY) license (<http://creativecommons.org/licenses/by/4.0/>).